A Proprioceptive Soft Tentacle Gripper Based on Crosswise Stretchable Sensors

Zhexin Xie, Feiyang Yuan, Zemin Liu, Zhaoning Sun, Elias M. Knubben, and Li Wen *, *Member, IEEE*

***Abstract*—Soft robotics have attracted growing attention due to their compliant structure, safe operation, and promising applications in constrained and unstructured environments. Octopus can employ its arm and suckers to catch prey in complex environments. Intrigued by these capabilities, we explored a new approach in sensing, modeling, and control of a bio-inspired soft robot that enables both bending and suction for manipulating and perception of environmental load. By implementing EGaIn based soft sensors with a crosswise manner on the soft tentacle, both sensory feedbacks of the elongation (EL) and expansion (EP) induced by the pneumatic inflation can be acquired. We built a variable curvature model for the bending kinematic reconstruction of the soft robot based on the feedback of the soft sensors. Both modeling and experimental results show that this crosswise sensor design allows for more accurate sensing of the soft robot's bending than the one-axis design. With the crosswise sensor, the robotic tentacle can distinguish the bending under external stimuli and internal self-actuation. We experimentally verified the sensory response as well as the accuracy of the self-sensing system and the model under freeload bending, externally loaded bending and grasping conditions. By synergistically adopting the sensing of the vacuum-actuated suckers with the bending arm, we show that the soft robot can detect, suck, and bend to grasp objects. The results from this research may provide new design and application insights into the creation of autonomous soft manipulators with both bending and suction for tasks in constrained environments.**

***Index Terms*—soft robotics, soft sensor, modeling and control, Soft Gripper**

I. Introduction

The creation of soft robots draws profound interest from scientific and engineering communities due to their safe human-robot interaction, large deformation, and easy to operate in environments [1]-[4]. However, achieving a controllable state of the large deformation of the soft robot remains challenging while taking the contact and disturbance of the environment into account. In nature, the octopus arm represents one great example that can conduct complex tasks in the constrained, low visibility underwater environment by adopting the sensory feedback of its tentacle skin and suckers [5][6]. Because of their flexibility, agility, and adaptability for efficiently manipulating in constrained environments, octopus arms give inspirations to the developments of several continuum manipulators, which allow for freeload motion control [7]-[15]. However, little is known regarding the modeling and control of the bending arm when considering bending under external loads and disturbance, and under grasping condition.

Soft sensors (such as EGaIn, and ionic polymer-metal composite) are a practical solution for soft robots to perceive and adapt to the environments [16]-[21]. Integrated flexible electronics (such as organic or inorganic flexible electronics) on the soft robots can further acquire the motion state of the soft robot [22]-[24]. These flexible sensors can offer feedback on the soft robots under large deformation as well as identify the motion of soft robots under different load conditions.

In the present work, we proposed a soft robotic tentacle with sensing of both bending and suction. In contrast to previous studies on octopus-inspired robots, which primarily focus on freeload modeling of arm motion [25]-[28], we focus on the (i) sensory-based bending model under both freeload and external stimuli and (ii) sensory-based autonomous manipulating strategy for constrained environments. We first design and fabricated the octopus inspired soft tentacle with sensing of bending and suction (Fig. 1(a)). Crosswise sensors were come up for accurate feedback of the expansion of the tentacle, a variable curvature kinematic model was established to reconstruct the bending profiles of the robotic tentacle. We found that the crosswise sensing system and the kinematic model can instantaneously track the bending states of the robotic tentacle under both freeload bending, load, and external obstructed conditions. With the crosswise EL-EP sensor, the robotic tentacle can distinguish the bending under external stimuli and internal self-actuation. After that, we demonstrate that the model can be accurately used during the grasping process to sense the enveloping of the object. Finally, we explored the application of our robotic tentacle system in confined environments. We demonstrated its ability to

This work was supported by the National Science Foundation support projects, China (Grant No. 61822303, 91848105, 61633004, 91848206), in part by National Key R&D Program of China (Grant No. 18YFB1304600 and 2019YFB1309600). (Corresponding author: Li Wen, email: liwen@buaa.edu.cn)

Z. Xie, F. Yuan, Z. Liu, Z. Sun and L. Wen are with School of Mechanical Engineering and Automation, Beihang University, Beijing 100191, China. (e-mail: zhexinxie@buaa.edu.cn, feiyangyuan_buaa@163.com, zeminliu@buaa.edu.cn, sunzhaoning1998@buaa.edu.cn, liwen@buaa.edu.cn)

E. M. Knubben is with Leitung Corporate Bionic Department, Festo SE & Co. KG, Esslingen 73734, Germany. (e-mail: elias.knubben@festo.com).

Z. Xie is also with Shenyuan Honors College, Beihang University, Beijing 100191, China.

L. Wen is also with Beijing Advanced Innovation Center for Biomedical Engineering, Beihang University, Beijing, China.

This article has been accepted for publication in a future issue of this journal, but has not been fully edited. Content may change prior to final publication. Citation information: DOI 10.1109/TMECH.2020.2993258, IEEE/ASME Transactions on Mechatronics

autonomously avoid obstacles, detect and bring back the object of interests based on the use of all the self-sensing, bending, and suction functionalities. This study not only sheds light on how the soft sensors can be used in modeling and control of soft robots under different load conditions but also new application cues for the realization of soft robots capable of performing tasks in confined environments.

II. Materials and Methods

A. System design and fabrication overview

Distinguished from traditional rigid robots, soft robots possess large deformation and body expansions, which reflect the load conditions of the robots. By sensing these expansions, we can not only learn the shape but also the actuation condition of the soft robots. To this end, we came up with a crosswise sensor design. The soft sensor is composed of two layers: EL(elongation) sensor and EP (expansion) sensor which is laid in a crosswise manner (Fig. 1(a)). The overlap area of the EL and EP sensors is designed to be quite small, occupying 15% of the whole area of EL sensor. Therefore, this design helps to reduce the coupling between the EL and EP sensors and acquire two-dimensional accurate sensing feedback. The fabrication procedure of the crosswise EL-EP sensor follows steps shown in Fig. 1(a): *1)* Firstly, silicone elastomer (Ecoflex 30) was poured into a 3D printed mold to fabricate the sensor substrate with unsealed channels; *2)* after the sensor substrate was cured, a spin coater was used to form a thin film of liquid elastomer, the cured sensor substrate was then put on the elastomer film to seal the sensor channels; *3)* after the sensor channels were sealed, Liquid metal (EGaIn) was injected into the channel and the sensor was cut into a cross shape. The design of the crosswise sensors can result in the accurate deformation of the tentacle robot. The integrated fabrication approach of the crosswise sensor ensures the orthogonal relationship of EP and EL sensors.

Inspired by the octopus tentacle, the soft tentacle with suckers is designed to be cone-shaped, which generates variable bending curvature when inflated and allows us to grasp a wide range of objects. The suckers were designed by mimicking the geometries of the *infundibulum* and *acetabulum* of *Octopus Vulgaris*. The fabrication procedure of the octopus-inspired soft robotic tentacle follows the multi-step molding and casting process shown in Fig. 1(b). All air tubes of the suckers are connected to a single-channel vacuum generator for simplicity and efficient suction (see Fig. 1(c)).

The crosswise EL-EP sensor and soft robotic tentacle were then integrated as Fig. 1(c) shows, three pieces of soft sensors are stuck on the ektexine of the bending actuator to acquire swelling information of the bending actuator. EL sensors were placed along the length of the bending actuator to sense the length change of the ektexine, while the EP sensors were circumferentially placed along the bending actuator to sense the perimeter change due to the expanding of the ektexine. As Fig. 1(c) inset panel shows, by sticking only both ends of each sensor on the bending actuator (red points in the figure), the inflation of the bending actuator only lead to EL sensors' elongation along the length and EP sensors' elongation along the perimeter of the bending actuator (Fig. 1(d)).

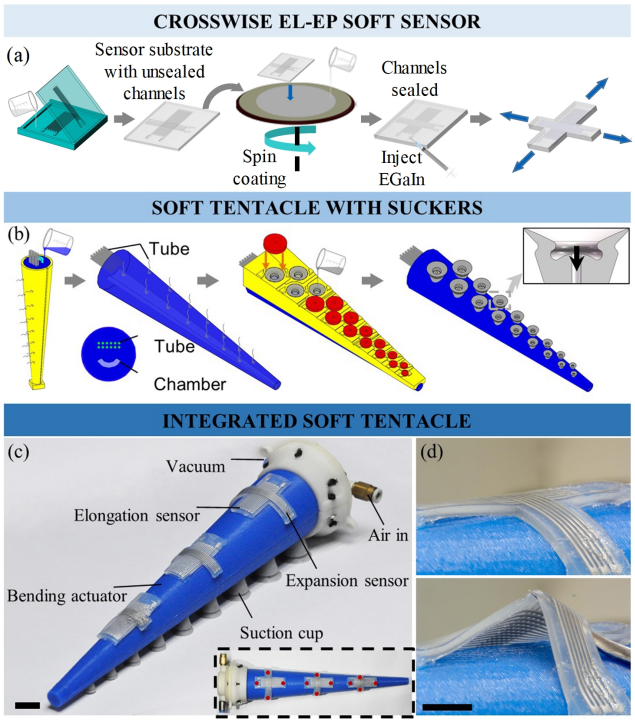

Fig. 1 Design and fabrication of the octopus-inspired soft robotic tentacle instructed by integrated EL (elongation) and EP (expansion) crosswise stretchable sensors. Step-by-step fabrication details of the **(a)** EL-EP sensors and **(b)** soft robotic tentacle. **(c)** Photograph of the integrated soft tentacle prototype. Three EL-EP sensors are attached to the surface of the actuator. Inset image: top view of the planform of the soft robotic tentacle, red points indicate the place where EL-EP sensors are glued on the bending actuator. Scale bar, 10mm. **(d)** EL-EP sensor is soft, stretchable, and bonded on the robotic tentacle with the four sites. Scale bar, 10mm.

B. Bending kinematics based on the crosswise EL-EP sensors

The bending kinematics presented is constructed as a function of the feedback of the soft sensors in a real-time manner. Inspired by the octopus arms (Fig. 2(a)), the tapered robotic tentacle is actuated to present a variable bending curvature along with the inner profile (Fig. 2(b), red line). In order to describe the variable curvature, we divide the robotic tentacle into three sections, the curvature of each section is calculated separately, for the *i-th* section ($i \in \{1,2,3\}$), the EL-*i* and EP-*i* sensors are used to sense the inflation. As shown in Fig. 2(b), the soft robotic tentacle considered in this study is cone-shaped with taper angle $\alpha = 9°$, length $L = 200$ mm and tip diameter $D_{tip} = 8.4$ mm. The scale parameters were designed for grasping daily items. The diameter $D(z)$ of the actuator at distance z $(0 < z < L)$ from the actuator's bottom is given as

$$D(z)=D_{tip}+2(L-z)\tan\frac{\alpha}{2}. \quad (1)$$

The position of the center point for the *i-th* sensor ($i = 1, 2, 3$, see black dots in Fig. 2(b)) is defined by coordinate z_i.

The modeling procedure consists of two steps, the first involves transforming between the soft sensors' electrical

This article has been accepted for publication in a future issue of this journal, but has not been fully edited. Content may change prior to final publication. Citation information: DOI 10.1109/TMECH.2020.2993258, IEEE/ASME Transactions on Mechatronics

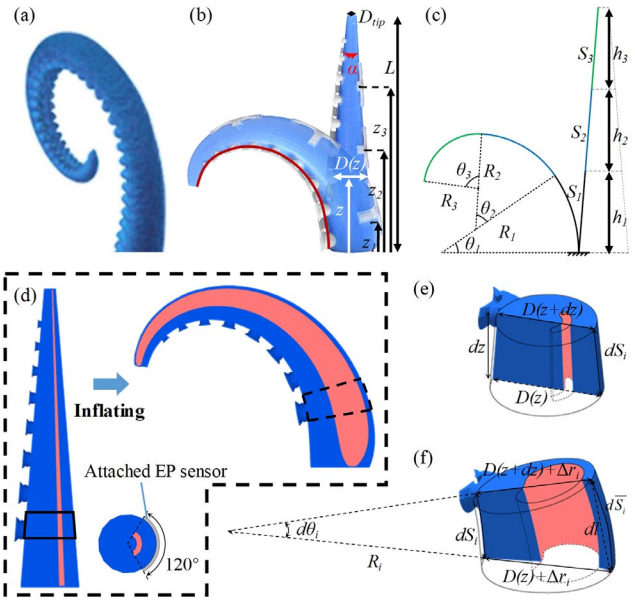

Fig. 2. Geometry and kinematics model of the soft robotic tentacle with EL-EP sensors. (a) The octopus arm bending with variable curvature. **(b)** The global view of robotic tentacle bending, the inner bending profile (in red) is analyzed. **(c)** General kinematics model for the robotic tentacle, three sections (i = 1, 2, 3) was divided based on the distribution of the three EL-EP sensors. **(d)** Schematic representation of the soft robotic tentacle's deformation. **(e)** and **(f)** represents the original and deformed shape of infinitesimal trapezoid element selected from **(d)**, respectively.

signals $\{\Delta R_{EL\text{-}i}, \Delta R_{EP\text{-}i}\}$ and inflation geometries $\{\overline{S_i}, \Delta r_i\}$ of the robotic tentacle ($\overline{S_i}$ indicates the length of the elongated ektexine of the *i-th* section and Δr_i indicates the radial expansion of the *i-th* section, which can derive from the EL-*i* and EP-*i* sensors, respectively); The second involves transforming between tentacle bending profile geometries $\{\theta_i, R_i\}$ and inflation geometries $\{\overline{S_i}, \Delta r_i\}$. To solve the second step, we fitted formulas based on the recorded results of experiments with the soft sensors. In order to simplify the model, we made the following assumptions:

i. For *i-th* section ($i \in \{1,2,3\}$), the bending profile of each had constant curvature, and the curves were tangent at the intersection points.
ii. For *i-th* section ($i \in \{1,2,3\}$), each point along the length of the tentacle's ektexine obtains the same elongation and expansion equal to the EL-*i* sensor's strain and EP-*i* sensor's strain, respectively.

1) *Characterization of the EP-EL sensors*

To solve the transforming between tentacle's inflation geometries and the EP-EL sensor's electrical signals, two series of experiments were conducted to evaluate the strain characterization of the EL-EP sensors. As the inset image of Fig. 3(a) shows, firstly, we test single sensor's uniaxial strain characterization, for each sensor (EL or EP), it was stretched along direction of the arrow; The second was to test the cross-impact between the EL and EP sensor, EP-3 was chosen to evaluate the impact from stretching of EL-3 (EP-3 obtains the shortest length and the EL-3's impact on it should be most obvious, relatively). We applied a controlled linear strain for each sensor using a commercial robotic arm (MOTOMAN

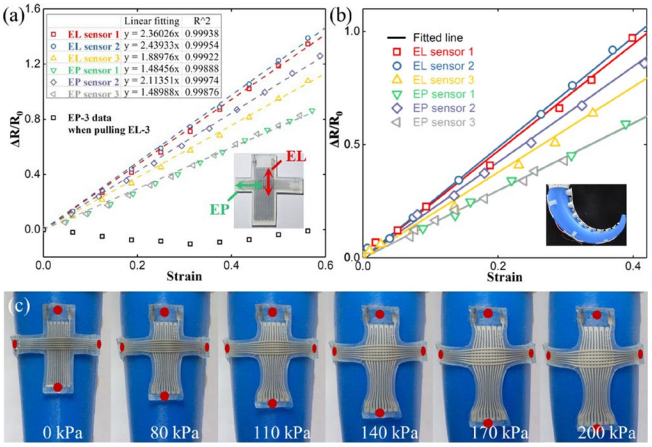

Fig. 3 EP-EL stretchable sensors characterization. (a) Relative change in resistance of the EL and EP sensors as a function of uniaxial longitudinal strain to 60% strain (surpass the maximum strain in this study). **(b)** The strain and corresponded resistant response of the EL-EP sensors on the bending actuator meets with the linearity shown in **(a)**. Inset panel shows the EL-EP sensors elongating with the bending of the soft robotic tentacle, the elongation of the EL-EP sensors was measured from the digital images. **(c)** The crosswise sensors were bonded on the robotic tentacle and elongated along with tentacle's inflation (with air pressure from 0-200kPa), the bonding sites are indicated in red.

MH3F, YASKAWA Inc., Japan), the change of the resistance of the sensor was recorded via precision multimeter (Fluke 8845A, Fluke Inc., USA).

Fig. 3(a) shows the uniaxial strain characterization of the six sensors. The inset table of Fig. 3(a) shows the linear fitting coefficient (k) and the determination coefficient R^2 of the sensors. The sensor's resistance change proportions $\Delta R/R_0$ of the sensors show a linearity relationship to the strain ε, as

$$\frac{\Delta R}{R_0} = k\varepsilon, \tag{2}$$

where R_0 denotes the original resistance of the sensor.

Furthermore, data of the cross-impact between the EL and EP sensor was shown with the black blocks, it can be seen that during the stretching of EL-3, the electrical signal of EP-3 shows little variation, which indicates that the cross-impact between the EL and EP sensor is negligible and we can treat the EL and EP sensors individually.

Now that we established the derivation of the sensor's deformation through the electrical signal, the robotic tentacle inflation geometries $\{\overline{S_i}, \Delta r_i\}$ can be acquired. Here we define the *i-th* EL/EP sensor's linear coefficient as $k_{EL\text{-}i}/k_{EP\text{-}i}$, then we have

$$\frac{\Delta R_{EL\text{-}i}}{R_{0,EL\text{-}i}} = k_{EL\text{-}i}\frac{\overline{S_i}\text{-}S_i}{S_i} \tag{3}$$

The inner chamber of the robotic tentacle has a β = 120° swept ring-shaped cross-section and has the same center point with the actuator cross-section. As a result, the EP sensors approximately measure 1/3 of the actuator circumferential length, we have

$$\frac{\Delta R_{EP\text{-}i}}{R_{0,EP\text{-}i}} = k_{EP\text{-}i}\frac{\pi\frac{\beta}{360}2\Delta r_i}{\pi\frac{\beta}{360}D(z_i)} = k_{EP\text{-}i}\frac{2\Delta r_i}{D(z_i)}, \tag{4}$$

where $D(z_i)$ is the actuator diameter at the place of the *i-th* sensor ($z = z_i$), which is defined by Eq. **1**.

We further validated the linear performance of the sensors after they were attached to the robotic tentacle. As Fig. 3(b) shows, the three sensors were attached to and stretched along with the bending of the robotic tentacle. The strains of the EL-EP sensors were captured by a camera and calculated in Matlab, and then plotted in Fig. 3(b) (as the scatters shows) with the corresponded resistance change proportions $\Delta R/R_0$. The solid lines in Fig. 3(b) indicates the fitted curves derive from Fig. 3(a). It can be seen that the sensors have the same linearity when deforming with the robotic tentacle, which confirmed that the calibrations of the sensors shown in Fig. 3(a) was able to be used in the sensing and modeling of the robotic tentacle. Fig. 3(c) shows the elongate state of the sensor when the robotic tentacle was inflated with pressure from 0-200kPa, the red dots indicate the bonding sites of the sensor.

2) Bending kinematics based on the crosswise EL-EP sensors

The resulting model structure of the proposed general kinematics according to assumptions i-ii are illustrated in Fig. 2(c). Table I lists important model parameters in this study.

As mentioned previously, the robotic tentacle was divided into three sections, as Fig. 2(c) shows, the *i-th* section has the vertical length of h_i and inner profile length S_i, we have

$$\sum_{i=1}^{3} h_i = L \tag{5}$$

and

$$h_i = S_i \cos\frac{\alpha}{2}. \tag{6}$$

After inflation, the *i-th* section bends into an arc with bending angle θ_i and bending radius R_i, we have

$$R_i\theta_i = S_i\ . \tag{7}$$

Fig. 2 provides a schematic representation of the soft robotic tentacle in both a neutral state and a bending state (Fig. 2(d)). Inserted inextensible soft tubes for the suckers have a greater elastic modulus than that of the bending actuator, makes the inner layer inextensible relative to the outer layer.

TABLE I
ACTUATOR PARAMETERS USED FOR MODELING

Parameter	Symbol	Value
Actuator length	L	200 mm
Taper angle	α	9°
Tip diameter	D_{tip}	8.4 mm
Section length	h_i	60 mm, 70 mm, 70 mm (i =1, 2, 3)
Sensor position	z_i	40 mm, 90 mm, 135 mm (i =1, 2, 3)

To understand the detailed deformation of the robotic tentacle, an infinitesimal trapezoid element of the *i-th* section in Fig. 2(d) with the height of dz was selected and analyzed, the original shape of the infinitesimal trapezoid element was shown in Fig. 2(e), the diameter of the top and the bottom of the trapezoid is $D(z)$ and $D(z+dz)$. After inflating, the element deformed into the shape shown as Fig. 2(f). The inner profile of the element bends into an arc with the infinitesimal bending angle $d\theta_i$ and radius R_i, without length changing (dS_i). We have

$$d\theta_i = \frac{dS_i}{R_i} = \frac{dz}{R_i\cos\frac{\alpha}{2}} \tag{8}$$

The outer layer of the element turns into an irregular arc as the function of the inflation. Elongation and radial expansion occurred on the right hypotenuse and were characterized as $d\overline{S_i}$-dS_i and Δr_i, respectively. The irregular arc length $d\overline{S_i}$ was approximated to its chord length $d\bar{l}$, which derives following the cosine law, as

$$d\overline{S_i} \approx d\bar{l} = \sqrt{\left(\overline{D}(z+dz)\right)^2 + \left(\overline{D}(z)\right)^2 - 2\overline{D}(z+dz)\overline{D}(z)\cos d\theta_i}, \tag{9}$$

here $\overline{D}(z) = R_i + D(z) + \Delta r_i$.

Let

$$f_i(z) = \frac{z}{R_i\cos\frac{\alpha}{2}} - \frac{R_i + \Delta r_i + D_{tip} + 2L\tan\frac{\alpha}{2}}{2R_i\sin\frac{\alpha}{2}}. \tag{10}$$

By combining Eqs. **6-9**, and using Taylor expansion

$$\cos d\theta_i = 1 - \frac{d\theta_i^2}{2} + o\left(d^2\theta_i\right), \tag{11}$$

here $o\left(d^2\theta_i\right)$ indicate infinitely small quantities of higher order than $d^2\theta_i$. We obtain

$$\begin{aligned} d\overline{S_i} &\approx 2\tan\frac{\alpha}{2}\sqrt{f_i(z)^2 + 1 + \frac{o\left(d^2z\right)}{d^2z}}\,dz \\ &\approx 2R_i\sin\frac{\alpha}{2}\sqrt{f_i(z)^2+1}\,df_i(z). \end{aligned} \tag{12}$$

Integrate both sides of the Eq. **12,** we obtain

$$\int d\overline{S_i} \approx \int 2R_i\sin\frac{\alpha}{2}\sqrt{f_i(z)^2+1}\,df_i(z)\,, \tag{13}$$

where

$$\overline{S_i} = g\left(f_i\right) = R_i\sin\frac{\alpha}{2}\left(f_i\sqrt{f_i^2+1} + \ln\left(f_i + \sqrt{f_i^2+1}\right)\right)\Bigg|_{f_i\left(\sum_0^{i-1}h_j\right)}^{f_i\left(\sum_0^{i}h_j\right)}, \tag{14}$$

in which we define $h_0 = 0$.

With Eq. **7** and Eq. **14**, the *i-th* segment's bending radius R_i and bending angle θ_i can derive from $\overline{S_i}$ and Δr_i. Eq. **14** represents the variable curvature model when considering both elongation and expansion (named VCEP for abbreviation) proposed in this study.

Meanwhile, when considering the previously studied approaches [7][8], which ignore the expansion (Δr_i), we have

$$\overline{S_i} = g(f_i')\Big|_{f_i'\left(\sum_0^{i-1}h_j\right)}^{f_i'\left(\sum_0^{i}h_j\right)}, \tag{15}$$

This article has been accepted for publication in a future issue of this journal, but has not been fully edited. Content may change prior to final publication. Citation information: DOI 10.1109/TMECH.2020.2993258, IEEE/ASME Transactions on Mechatronics

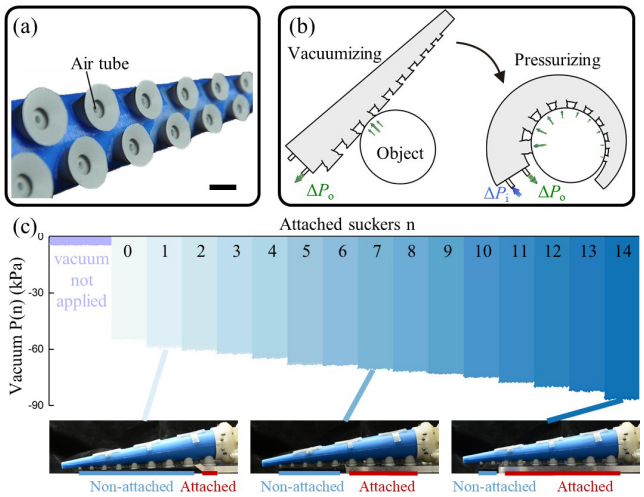

Fig. 4 Suckers' sensing of the soft robotics tentacle. (a) Two rows of suction cups are fabricated on the tapered soft actuator; silicone air tubes are inserted inside of the suction cups for vacuum-suction. Scale bar, 10mm. **(b)** Suction-bending gripping principal of the robotic tentacle, firstly vacuum is applied, and some of the suckers get attached to objects. Once the attachment is detected, the tentacle is inflated to bend to wrap around objects. **(c)** The vacuum pressure of the suction cup array depends on the number of attached suckers.

where f_i' derives from the expression f_i after deleting the part of Δr_i, as

$$f_i'(z)=\frac{z}{R_i\cos\frac{\alpha}{2}}-\frac{R_i+D_{tip}+2L\tan\frac{\alpha}{2}}{2R_i\sin\frac{\alpha}{2}}. \tag{16}$$

Without considering expansion, Eq. **15** represents the variable curvature model when considering elongation only (we name this as VCE for abbreviation). We later evaluate the VCEP model based on Eq. **14** and the VCE model based on Eq. **15** in section IIIA.

C. *Sensing and modeling of the suction cups*

Owning to the application of vacuum inside the suckers (Fig. 4(a)), the robotic tentacle was able to detect and grasp the object following the process shown in Fig. 4(b): *i)* firstly vacuum was applied to the suckers; *ii)* once sucker attached to object and the pressure inside the sucker changed, the tentacle was inflated to bend; *iii)* the tentacle keep on bending to wrap around the object, and more suckers get attached to the object to achieve stable grasping. Vacuum pressure was measured to detect the attachment of the suckers. Because all suckers were connected, give the constant vacuum input, the vacuum pressure (P(n)) changed only with the number (n) of attached suckers. As Fig. 4(c) shows, the tentacle was actuated to attach to the acrylic plate, with the number of attached suckers increase, the vacuum pressure increase. By measuring the vacuum pressure inside the suckers, the tentacle was able to sense the attachment of objects.

III. Results

A. *Sensory feedback of the robotic bending under freeload and load conditions*

We first evaluate the performance of the sensor system and the accuracy of the VCEP model, we conducted experiments on the freeload motion of robotic tentacle. The robotic tentacle was inflated with pressures starting from 0 kPa to 200 kPa with an interval of 15 kPa. The pressure was controlled by the electro-pneumatic proportional pressure valve (ITV0030, SMC, Japan). The bending configurations at different pressures were then captured (see Fig. 5(a)) and treated in MATLAB to extract the experimental inner bending profiles of the robotic tentacle. Meanwhile, the three EL sensors and three EP sensors were connected in series to gather the electrical signal feedback. A constant current of 50 mA was applied to the circuit and a NI data acquisition board (PCI-6284, National Instruments, USA) was used to record the relative voltage increment of each sensor simultaneously, the resistant change $\{\Delta R_{EL\text{-}i}, \Delta R_{EP\text{-}i}\}$ were then calculated via the voltage data. By using VCEP model based on Eqs. **3, 4** and **14**, we calculated the actuator's bending parameters $\{\theta_i, R_i\}$, with the bending parameters, the bending profile was reconstructed.

Fig. 5(b) shows the comparisons between experimental

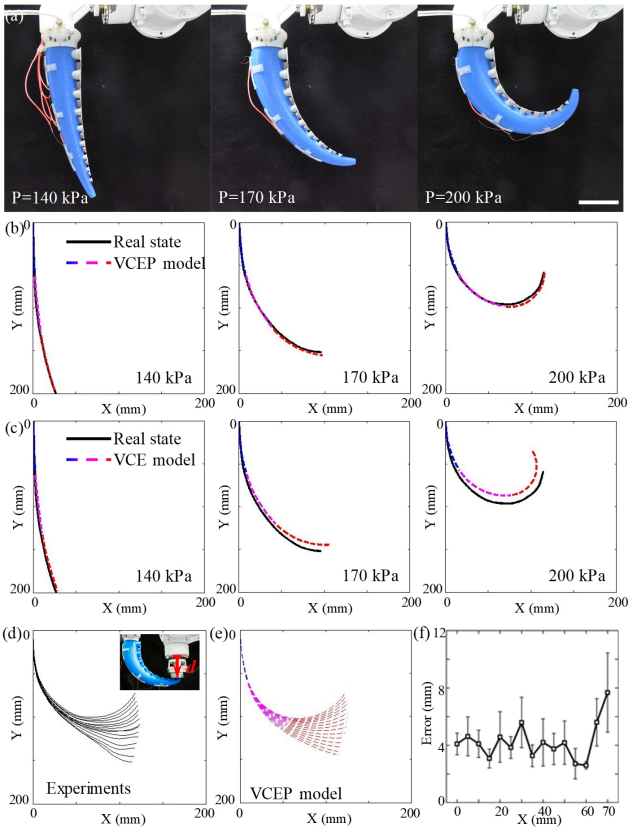

Fig. 5 Comparisons of robotic tentacle bending between model and experiments. (a) Images of the soft robotic tentacle inflated at 140 kPa, 170 kPa, and 200 kPa. Scale bar, 50mm. **(b)** Corresponded bending profile comparison between experiment (solid lines) and VCEP model reconstruction (dash lines). **(c)** Corresponded bending profile comparison between experiment (solid lines) and VCE model reconstruction (dash lines). **(d)-(f)** Evaluation of the robotic tentacle's bending model (VCEP) under different loads: **(d inset panel)** images of the loading process, the robotic tentacle was inflated with the air pressure of 200 kPa, and the tip of the robotic tentacle was pressed vertically with the distance *d* by a programmed robotic arm. Bending profiles extracted from the images **(d)** and VCEP model calculated bending profiles **(e)** and their tip points' coordinate errors **(f)**. Number of experimental repetitions: $N = 3$.

This article has been accepted for publication in a future issue of this journal, but has not been fully edited. Content may change prior to final publication. Citation information: DOI 10.1109/TMECH.2020.2993258, IEEE/ASME Transactions on Mechatronics

(black solid lines) and model reconstructed bending profiles of the actuator (dash lines), for the model reconstructed bending profiles, the blue, pink and red parts represented the three circular sections of the whole variable curvature bending profile. It can be seen that at pressure from 0-200 kPa, the VCEP model reconstructed bending profiles fit pretty well with the reality. Moreover, the VCE model reconstructions were also compared here as Fig. 5(c) shows. It can be seen that at the same actuated state, the bending profile reconstructed by the VCE model bends more than that of the VCEP model and the experimental, and the error increased with the air pressure. It indicated that the model is precise when both the elongation ($\overline{S_i}$) and expansion (Δr_i) were taken into account.

Then, we investigated the performance of the VCEP model under load conditions. The robotic tentacle was fixed at its base vertically and actuated at a pressure of 200 kPa, one plate was mounted on the commercial robotic arm and programmed to move vertically to press the tip of the actuator (as Fig. 5(d) inset panel shows). The tip of the actuator was pressed with a distance of 0-70 mm, with an interval of 5 mm. For each press distance, the tracked bending profile of the actuator (Fig. 5(d)) was compared with the bending profile based on the VCEP model (Fig. 5(e)). We calculate the position error of the bending profiles' tip point between experimental and model reconstructed. The position error as the function of press distance was shown in Fig. 5(f). It can be seen that the error was smaller than 10 mm as the press distance changed.

B. Soft robotic tentacle under external stimuli

To demonstrate the utility of the VCEP model and the feedback of soft sensors, we evaluate the performance of the robotic tentacle under external stimuli in both pressurized and unpressurized states.

Firstly, the robotic tentacle was deformed to a similar bending profile by external stimuli and internal actuation (200 kPa), as shown in Fig. 6(a) and (d). Fig. 6(c) and (f) show the electrical signals of the EL-EP sensors during the two processes. From Fig. 6(c) and 7(f), the ΔR of EL sensors raise substantially in both processes; however, the EP sensors fall slightly under external stimuli but raise notably under self-actuation by pressurization. Secondly, Fig.6(g) shows the process of applying external stimuli to the actuated tentacle (200 kPa). It can be seen from 6(i) that we can identify the external stimuli with the performance that EL sensors fall obviously while the EP sensors raise slightly.

The VCEP model-based bending curve was calculated and compared with the extracted experimental bending profile in Fig. 6(b), 6(e), and 6(h) for all the three processes in Fig. 6(a), 6(d), and 6(g), respectively. The model fits well with the experimental profiles of the robot under external stimuli in both pressurized and unpressurized states.

C. Autonomous grasping via sensory feedback of bending and suction

To evaluate the grasping performance of the VCEP model and the robot in the real world, we used the robotic tentacle to grip an apple by inflating the robot with pressure from 0 kPa to 260 kPa. The apple was kept in place on the table, and the robot was inflated to 260 kPa step by step with an interval of 20 kPa (Fig. 7(a) upper row), ΔR of each sensor is plotted as a function of time in Fig. 7(b) during this process. The bending profile of the tentacle was tracked with a camera and plotted together with a bending profile reconstructed based on the VCEP model as Fig. 7(a) (lower row) shows. Furthermore, maximum inscribed circles of the model constructed bending profiles were calculated and plotted to roughly feedback the size of the object enveloped in the bending profile, as shown with the dashed circle in Fig. 7(a). The curvature of the maximum inscribed circle (ε_m) is plotted as a function of pressure in Fig. 8. It should be noted that as the snapshots in Fig. 7(a) shows, the robot fitted the object best under pressure P = 220 kPa. When the pressure is higher than 220 kPa (i.e., 240 kPa and 260 kPa), the robotic tentacle over-bent and led to the detachment of a few suckers, as called "over-enveloped". It can be seen that before the robotic tentacle

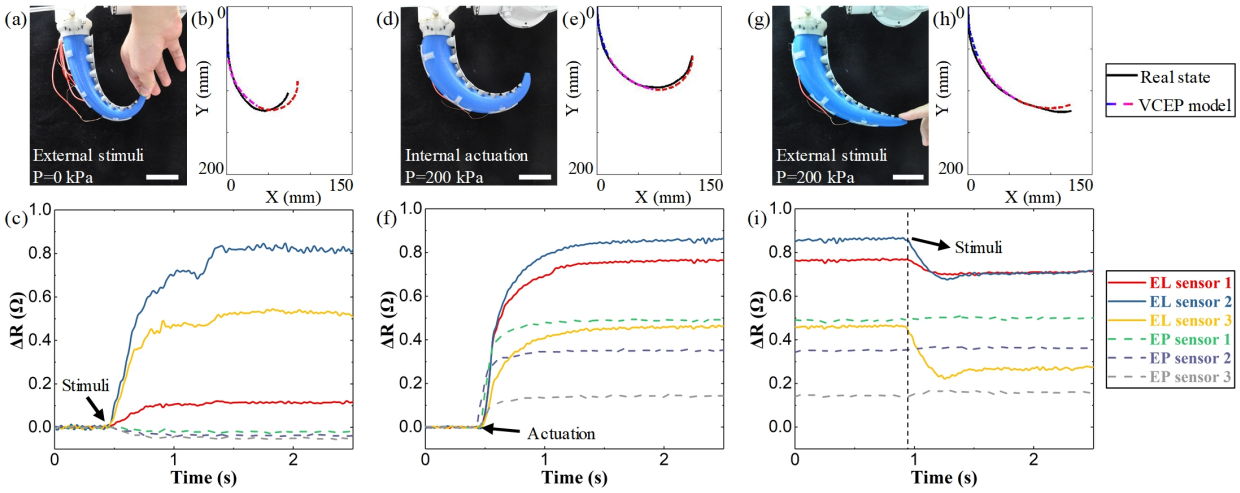

Fig. 6 Robotic tentacle feeling the external stimuli under both pressurized and unpressurized states. The robotic tentacle was deformed to similar bending profile respectively by external stimuli **(a)** and internal actuation **(d),** and then another external stimuli was applied to pressurized tentacle **(g).** Corresponding electrical signals of the EL-EP sensors of the **(a)**, **(d)** and **(g)** process were shown as **(c)**, **(f)** and **(i)**, and the VCEP model matches well with corresponded processes **(b, e** and **h)**. Scale bar, 50mm.

This article has been accepted for publication in a future issue of this journal, but has not been fully edited. Content may change prior to final publication. Citation information: DOI 10.1109/TMECH.2020.2993258, IEEE/ASME Transactions on Mechatronics

enveloped the object (P < 220 kPa), for both EL and EP sensors, ΔR increased step by step with the pressure increase (Fig. 7(b)). What makes sense is that in the "over-enveloped" states (P > 220 kPa), although the out layer of the tentacle kept on expanding and ΔR of the EL and EP sensors continue increasing with pressure, the VCEP model-based bending profiles still meet the realities well, as Fig. 7(a) shows. The maximum inscribed circle kept almost constant as the pressure increases, which can be recognized as a "stop signal" of the grasping process. The grasping status was determined as $\{\theta_i, R_i\}$ kept constant and P(n) guarantied the stable suction.

After the grasping performance evaluation, we explored the application of our robotic tentacle system at the constrained environment and demonstrated its ability to smartly avoid obstacles, detect and bring back the object of interests, based on the use of all the sensing, bending and suction functionalities (Fig. 8 and SI video). Specially, the robotic tentacle was mounted on the commercial robotic arm and moved by following its own instructions to get around of soft/rigid barriers and then went through a hole to find and fetch the target object. In this example, the real-time bending profile was shown as Fig. 8(d)), the VCEP-calculated bending curvatures (Fig. 8(a)), and the vacuum signal of the suckers (Fig. 8(b)) as a function of time was shown. The grasp process was divided into three steps (S_{Barr}, S_{Detec} and S_{Grab}):

(*i*) S_{Barr}: Starting with the non-pressurized tentacle (0 s) the robotic arm was instructed to move forward, when the tentacle contacted with the soft barrier, ΔR of the sensors changed and the curvature of the tentacle started to increase,

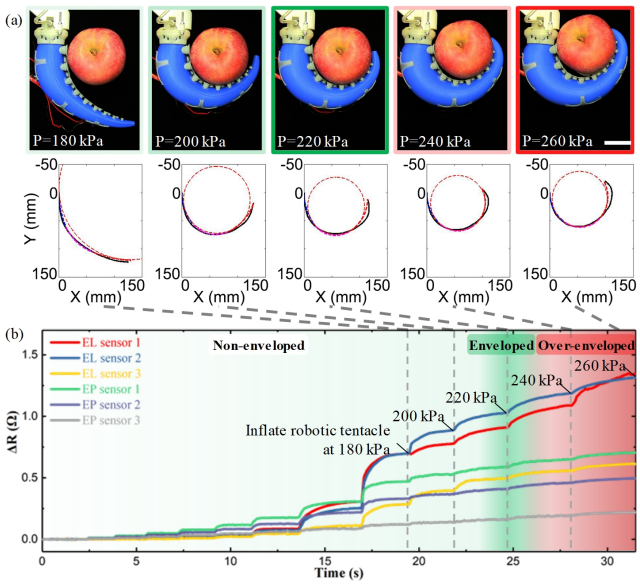

Fig. 7 Robotic tentacle grasped an object and can recognize the grasping state based on the sensory feedback of both bending and suction. (a) (Upper) Images of the grasping sequence between an apple and the soft robotic tentacle, (lower) corresponded bending profile comparison: bending profiles extracted from the images (black solid line), VCEP model calculated bending profiles and its maximum inscribed circle (dash line). Scale bar, 50mm. (b) ΔR of each sensor as a function of time during the grasping process, pressure was added steeply from 0 kPa to 260 kPa with an interval of 20 kPa, the grasping process was divided into three stage: non-enveloped (P < 220 kPa, time sequence shown with light green background), enveloped (P = 220 kPa), grasped (*P* = 220 kPa, green background) and over-enveloped (P > 220 kPa, red background).

once the max value of $\{\varepsilon_1, \varepsilon_2, \varepsilon_3\}$ raised up to a given threshold curvature ε_0 (Fig. 8(a)), robotic arm stopped (12.6 s) and went backward. The robotic arm moved laterally to evade the soft barrier and then sensed the rigid barrier in the same manner (21.5 s). The time spent to evade the rigid barrier was seen less than the soft barrier, which indicates that the robotic tentacle can detect barriers' softness with the different behavior of the sensors.

(*ii*) S_{Detec}: The robotic arm moved laterally again and kept going forward till the whole robotic tentacle got inside the hole without any disturbance (35 s), in this step, a constant vacuum was applied to suckers for object detection, and the pressure turned from just below 0 to -60 kPa (Fig. 8(b)). After getting inside the hole, the robotic arm was firstly turned right and inflated up to 260 kPa, trying to fetch objects (68.5 s). During the inflating process, the suckers' pressure did not change and the curvatures $\{\varepsilon_1, \varepsilon_2, \varepsilon_3\}$ were found to increase continuously without leveling off to constant (Fig. 8(a)). This indicated no objects on the right side. The robotic tentacle was then turned left for further detection (74 s).

(*iii*) S_{Grab}: The robotic tentacle was moved slowly with vacuum applied to the suckers, once some of the suckers got attached to objects, the vacuum pressure P(n) went down rapidly to -80 kPa (Fig. 8(b)) and the robotic tentacle was inflated to grasp the detected object (86.6 s). During the grasping process, more suckers engaged with the surface of the object and the vacuum pressure P(n) went down (Fig.8(b)), then the suckers can stick and help to hold the object in place and prevent slipping along the tentacle. The curvatures $\{\varepsilon_1, \varepsilon_2, \varepsilon_3\}$ firstly increased and then leveled off to constant, the pressure then stopped increasing, which means the object's grasping finished (118s). After finding the object grasped, the robotic tentacle was moved out of the hole with the object carried (130 s). When the object was gripped tightly, the bending sensor data stop changing; the sucker sensing can help to identify if the object was under a stable grasped state.

Based on the EL-EP sensory feedback and VCEP model, the detecting and fetching motion in an unconstructed environment could be utilized autonomously.

IV. Discussion and Conclusion

This article presents the design, modeling, and simple control of a new octopus inspired robotic tentacle that combines both bending and suction. The result shows that when considering both elongation and expansion of soft robot, the kinematics model achieved more accurate construction of the bending state of the robotic tentacle than considering elongation only. The design of the EP-EL sensor increases the redundancy of the sensing system, thus allows for accurate sensing when the robot is underload and disturbed. Compared to some previous studies that use smart sensors to recognize the robots' motions [19][20], the EP-EL sensors can accurately reflect the bending state of the soft robot regarding both bending and expansion. The EL-EP crosswise sensor endows the robotic tentacle to identify the external stimuli at both pressurized and unpressurized states. The robotic

This article has been accepted for publication in a future issue of this journal, but has not been fully edited. Content may change prior to final publication. Citation information: DOI 10.1109/TMECH.2020.2993258, IEEE/ASME Transactions on Mechatronics

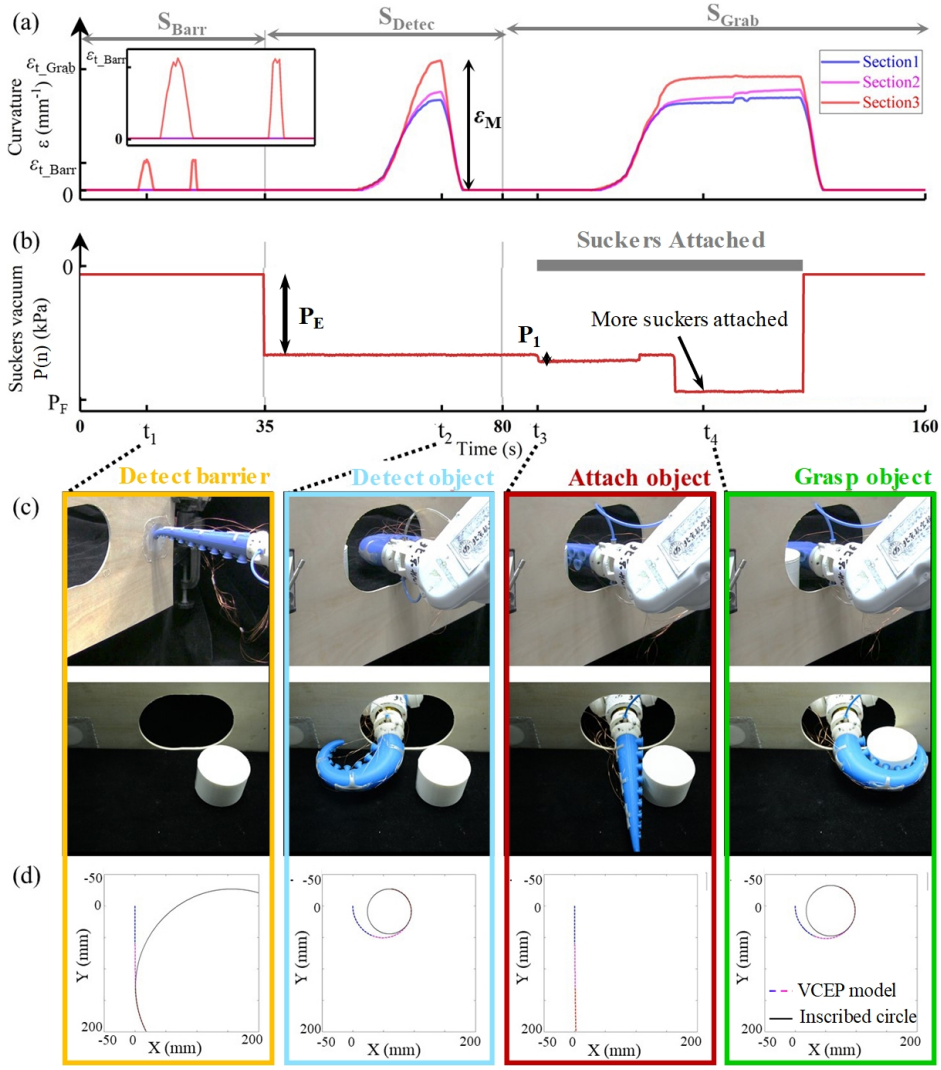

Fig. 8 The robotic tentacle autonomous went across a hole and fetch object in three steps: S_{Barr} – recognize and avoid the barriers, S_{Detec} - detect the object and S_{Grab} - grab and take out the object. (a) The VCEP-calculated bending curvatures of the three sections of the robotic tentacle, **(b)** the vacuum signal of the suckers during the process was plotted as a function of time. **(c)** and **(d)** the robotic tentacle snapshots and the modeled bending states during the grasping process. The progress was shown as SI video.

tentacle can also distinguish the bending under external stimuli and internal self-actuation.

Base on the feedback of the sensor, we developed a variable curvature kinematics model and evaluated its accuracy over the status of freeloading, underload, and interacting with the environment. In contrast to existing models aim to compensate for the open-loop prediction of the robots' actuation under specific manipulating environments (for example, extra gravity derived from multi-segment [29][30], underwater buoyancy [31], and the burden when carrying objects [32]). The VCEP model proposed in this article is based on the feedback of soft sensors. The crosswise sensing system enables manipulating not only at freeloading or underload but also when carrying objects. Meanwhile, by using the sensors, the VCEP model can be applied to guide the closed-loop control of the robot. The robotic tentacle with a kinematic model based on the feedback of soft sensors is an intriguing and potentially useful way to be extensively applied under a wide range of load conditions.

The VCEP model and suction pressure were seen to play essential roles in the detection and recognizing of objects and could be employed to close-loop grasping operation. As a result, the robotic tentacle can easily detect and avoid obstacles without the help of external vision [29][33]. It should be noted that both the bending of the robotic tentacle and the suckers offer the capability to detect objects, the overlaps of these two parts help to accurately detect target objects and contact of the environment, as well as manipulate under external forces from gravity or human interactions. This self-sensing, state reconstructing, and multi-sensing capabilities thus enable the robotic tentacle to perform tasks in visionless, narrow, and constrained environments (Fig. 8(d) and SI movie).

Regarding the limitation of the current prototype, our sensing system applies exposed wires for sensor data collecting, which may lead to a disturbance with the environment. Future studies could incorporate wireless modules for data processing. It should be noted that for these soft manipulators connected by several individual actuators, the kinematic model was usually divided by the number of

actuators [30][31][34]. In this article, we proposed a similar treatment of dividing the model into three segments for the continuous robotic tentacle. Ideally, the model accuracy can be improved by increasing the number of divided segments; however, increased complexity of modeling and fabrication would be accomplished. Therefore, there is a trade-off of the number of segments to divide the robot. For our robotic tentacle with a length of 20cm, we find that the kinematic model with three segments performs well when grasping daily objects. We imagine that the sensor system and variable curvature model could be further enhanced in the future for more accurate modeling [35]. Meanwhile, in the current study, we measured the vacuum pressure to detect the attachment of the suckers. We imagine that the soft suckers' sensory could be more intelligent and biologically relevant to the natural octopus suckers, tactile sensors are supposed to be added for more accurate dynamics modeling and grasping control.

REFERENCES

[1] M. M. Hamedi, V. E. Campbell, P. Rothemund, F. Güder, D. C. Christodouleas, J. F. Bloch, and G. M. Whitesides, Electrically activated paper actuators. *Advanced Functional Materials*, 26(15), 2446-2453, 2016.

[2] B. Mosadegh, P. Polygerinos, C. Keplinger, S. Wennstedt, R. F. Shepherd, U. Gupta, and G. M. Whitesides, Pneumatic networks for soft robotics that actuate rapidly. *Advanced functional materials*, 24(15), 2163-2170, 2014.

[3] L. Hines, K. Petersen, G. Z. Lum, and M. Sitti. Soft actuators for small-scale robotics. *Advanced materials*, 29(13), 1603483, 2017.

[4] P. Polygerinos, N. Correll, S. A. Morin, B. Mosadegh, C. D. Onal, K. Petersen, and R. F. Shepherd. Soft robotics: Review of fluid-driven intrinsically soft devices; manufacturing, sensing, control, and applications in human-robot interaction. *Advanced Engineering Materials*, 19(12), 1700016, 2017.

[5] P. P. C. Graziadei, and H. T. Gagne. Sensory innervation in the rim of the octopus sucker. *Journal of morphology*, 150(3), 639-679, 1976.

[6] F. Grasso, and M. Wells. Tactile Sensing in the Octopus. In: Prescott T., Ahissar E., Izhikevich E. (eds) Scholarpedia of Touch. Scholarpedia. Atlantis Press, Paris, 2016.

[7] M. Calisti, M. Giorelli, G. Levy, B. Mazzolai, B. Hochner, C. Laschi, and P. Dario. An octopus-bioinspired solution to movement and manipulation for soft robots. *Bioinspiration & biomimetics*, 6(3), 036002, 2011.

[8] B. Mazzolai, L. Margheri, M. Cianchetti, P. Dario, and C. Laschi. Soft-robotic arm inspired by the octopus: II. From artificial requirements to innovative technological solutions. *Bioinspiration & biomimetics*, 7(2), 025005, 2012.

[9] C. Laschi, M. Cianchetti, B. Mazzolai, L. Margheri, M. Follador, and P. Dario. Soft robot arm inspired by the octopus. *Advanced Robotics*, 26(7), 709-727, 2012.

[10] Z. Xie, A. G. Domel, N. An, C. Green, Z.Gong, T. Wang, E. M. Knubben, J. C. Weaver, K. Bertoldi, and L. Wen. Octopus Arm-Inspired Tapered Soft Actuators with Suckers for Improved Grasping. *Soft Robotics*, 2020.

[11] M. Giorelli, F. Renda, M. Calisti, A. Arienti, G. Ferri, and C. Laschi. Learning the inverse kinetics of an octopus-like manipulator in three-dimensional space. *Bioinspiration & biomimetics*, 10(3), 035006, 2015.

[12] M. D. Grissom, V. Chitrakaran, D. Dienno, M. Csencits, M. Pritts, B. Jones, and I. Walker. Design and experimental testing of the octarm soft robot manipulator. In Unmanned Systems Technology VIII (Vol. 6230, p. 62301F). *International Society for Optics and Photonics*, 2006.

[13] Walker I D, Dawson D M, Flash T, et al. Continuum robot arms inspired by cephalopods. Unmanned Ground Vehicle Technology VII. International Society for Optics and Photonics, 2005, 5804: 303-315.

[14] M. Cianchetti, M. Calisti, L. Margheri, M. Kuba, and C. Laschi. Bioinspired locomotion and grasping in water: the soft eight-arm OCTOPUS robot. *Bioinspiration & biomimetics*, 10(3), 035003, (2015).

[15] R. K. Katzschmann, A. D. Marchese, and D. Rus. Autonomous object manipulation using a soft planar grasping manipulator. *Soft Robot*, 2(4): 155-164, 2015.

[16] B. A. Gozen, A. Tabatabai, O. B. Ozdoganlar, and C. Majidi. High-density soft-matter electronics with micron-scale line width. *Advanced materials*, 26(30), 5211-5216, (2014).

[17] J. W. Boley, E. L. White, and R. K. Kramer. Mechanically sintered gallium–indium nanoparticles. *Advanced Materials*, 27(14), 2355-2360, 2015.

[18] Y. L. Park, B. R. Chen, and R. J. Wood. Design and fabrication of soft artificial skin using embedded microchannels and liquid conductors. *IEEE Sensors Journal*, 12(8), 2711-2718, 2012.

[19] G. Gerboni, A. Diodato, G. Ciuti, M.,Cianchetti, and A. Menciassi. Feedback control of soft robot actuators via commercial flex bend sensors. *IEEE/ASME Transactions on Mechatronics*, 22(4), 1881-1888, 2017.

[20] A. Atalay, V. Sanchez, O. Atalay, D. M. Vogt, F. Haufe, R. J. Wood, and C. J. Walsh, Batch fabrication of customizable silicone-textile composite capacitive strain sensors for human motion tracking. *Adv. Mater. Tech.* 2, 1700136, 2017.

[21] R. L. Truby, M. Wehner, A. K. Grosskopf, D. M.Vogt, S. G. Uzel, R. J. Wood, and J. A. Lewis. Soft somatosensitive actuators via embedded 3D printing. *Adv. Mater.* 30, 1706383, 2018.

[22] K. Sim, Z. Rao, Z. Zou, F. Ershad, J. Lei, A. Thukral, and C. Yu. Metal oxide semiconductor nanomembrane–based soft unnoticeable multifunctional electronics for wearable human-machine interfaces. *Science Advances*, 5(8), eaav9653, 2019.

[23] Y. Lee, M. Kim, Y. Lee, J. Kwon, Y. L. Park, and D. Lee. Wearable finger tracking and cutaneous haptic interface with soft sensors for multi-fingered virtual manipulation. *IEEE/ASME Transactions on Mechatronics*, 24(1), 67-77, 2018.

[24] C. Larson, B. Peele, S. Li, S. Robinson, M. Totaro, L. Beccai, and R. Shepherd. Highly stretchable electroluminescent skin for optical signaling and tactile sensing. *Science*, 351(6277), 1071-1074, 2016.

[25] S. Zhuo, Z. Zhao, Z. Xie, Y. Hao, Y. Xu, T. Zhao, H. Li, E. M. Knubben, L. Wen, L. Jiang and M. Liu. Complex multiphase organohydrogels with programmable mechanics toward adaptive soft-matter machines. *Science advances*, 6(5), eaax1464, 2020.

[26] Z. Gong, J. Cheng, X. Chen, W. Sun, X. Fang, K. Hu, and L. Wen. A Bio-inspired Soft Robotic Arm: Kinematic Modeling and Hydrodynamic Experiments. *Journal of Bionic Engineering*, 15(2), 204-219, 2018.

[27] T. Mahl, A. Hildebrandt, and O. Sawodny. A variable curvature continuum kinematics for kinematic control of the bionic handling assistant. *IEEE transactions on robotics*, 30(4), 935-949, 2014.

[28] B. Pawlowski, J. Sun, J. Xu, Y. Liu, and J. Zhao. Modeling of Soft Robots Actuated by Twisted-and-Coiled Actuators. IEEE/ASME Transactions on Mechatronics, 24(1), 5-15, 2018.

[29] A. D. Marchese, and D. Rus, "Design, kinematics, and control of a soft spatial fluidic elastomer manipulator," *Int. J. Robot. Res*. 35, 840-869, 2016.

[30] R. J. Webster III, B. A. Jones. Design and kinematic modeling of constant curvature continuum robots: A review. *Int. J. Robot. Res.* 29(13), 1661-1683, 2010.

[31] F. Xu, H. Wang, K. W. S. Au, W. Chen, and Y. Miao. Underwater dynamic modeling for a cable-driven soft robot arm. *IEEE/ASME Transactions on Mechatronics*, 23(6), 2726-2738, 2018.

[32] J. Wang, Y. Fei, and W. Pang. Design, Modelling and Testing of a Soft Pneumatic Glove with Segmented PneuNets Bending Actuators. *IEEE/ASME Transactions on Mechatronics*, 24(3), 990-1001, 2019.

[33] R. B. Scharff, R. M. Doornbusch, E. L. Doubrovski, J. Wu, J. M. Geraedts, and C. C. Wang. Color-Based Proprioception of Soft Actuators Interacting with Objects. *IEEE/ASME Transactions on Mechatronics*, 24(5), 1964-1973, 2019.

[34] V. Falkenhahn, T. Mahl, A. Hildebrandt, R. Neumann, and O. Sawodny. Dynamic modeling of bellows-actuated continuum robots using the Euler–Lagrange formalism. *IEEE Transactions on Robotics*, 31(6), 1483-1496, 2015.

[35] Y. Kim, G. A. Parada, S. Liu and X. Zhao. Ferromagnetic soft continuum robots. *Sci. Robot.* 4(33), eaax7329, 2019.